Atomistic Asymmetric Effect on the Performance of HfO₂-Based Ferroelectric Tunnel Junctions

Junbeom Seo[●] and Mincheol Shin[*]

School of Electrical Engineering, Korea Advanced Institute of Science and Technology, Daejeon, South Korea

We investigate the effects of atomistic interfaces on the device performance of HfO₂-based ferroelectric tunnel junctions (FTJs) using density-functional calculations. The atomistic structures of HfO₂ FTJs with different interfacial conditions are constructed and their device performances, such as *on*:*off* current ratio are evaluated. We find that without the external effects such as dissimilar metal electrodes or composite layers inserted to make an asymmetric potential barrier, the intrinsic effects stemming from the interface dipoles can be tailored toward achieving high device performance. Especially, the atomistic asymmetry effect, which gives the same effect as the built-in electric field, can be exploited for a high *on*:*off* current ratio at low external bias voltages. We demonstrate that the asymmetrically terminated Zr-doped HfO₂ FTJ exhibits a current ratio of 12, which is higher than any previously reported values, theoretically or experimentally, for HfO₂-based FTJs with symmetric metal electrodes.

I. INTRODUCTION

The ferroelectric (FE) tunnel junction (FTJ) has attracted much attention as one of the emerging nonvolatile-memory and neuromorphic devices owing to its scalability and high speed [1–5]. A typical FTJ incorporates a ferroelectric thin film sandwiched between two metal electrodes. Unlike the ferroelectric capacitor, the FTJ is a resistive-type memory device, and the resistance of the FTJ is changed with the polarization reversal by which the tunneling barrier is modulated. To utilize the tunneling electroresistance effect in practical applications, a large *on*:*off* current ratio is required. For this purpose, recent research has focused on device engineering such as modulation of the tunneling barrier by asymmetric metal electrodes or semiconducting electrodes [6,7] and insertion of a ferroelectric/dielectric composite barrier layer [8] as well as material engineering to improve the ferroelectricity [2].

In early experimental studies, FTJs with perovskite oxide ferroelectric films such as BaTiO₃, PbZr$_x$Ti$_{1-x}$O₃, and BiFeO₃ were reported [9–11]. While these materials are incompatible with the commercial complementary-metal-oxide-semiconductor (CMOS) process, the recent discovery of the ferroelectric phase (orthorhombic structure $Pca2_1$) in Si-doped HfO₂ has provided a breakthrough for ferroelectric-based electronic devices [12]. Ferroelectric HfO₂ can maintain outstanding ferroelectricity in

thicknesses of a few nanometers and has good compatibility with CMOS technology [13–17]. With these advantages of HfO₂, the feasibility of HfO₂-based FTJs has been reported [6,8,18–23].

HfO₂ FTJs, however, have shown a low *on*:*off* current ratio compared with perovskite oxide–based FTJs [5]. To increase the *on*:*off* current ratio, a deeper understanding of the interface between ferroelectric HfO₂ and metal electrodes is needed. The motivation comes from recent studies showing that the polar interface of perovskite oxide–based FTJs can significantly change the properties of the tunneling barrier with increase of the current ratio [24,25]. For HfO₂ FTJs, Hf or O polar surfaces of HfO₂ can be formed on the (001) surface. The polar interfaces may play a key role in the design of HfO₂-based FTJs with a sizable *on*:*off* ratio.

In this work, we investigate the atomistic-level interface effects on the device performances, which has not been done previously. Using density-functional-theory calculations, we construct atomistic device structures based on HfO₂ and Zr-doped HfO₂ (HZO) thin layers with various atomic interfaces. The motivation of considering HZO layers is that it has been reported that the performance can be improved by doping HfO₂, with the Zr atom being one of the widely used dopants for HfO₂ [26,27]. Also, we expect that HZO can provide variety in interface conditions, widening the room for device engineering toward increase of the *on*:*off* ratio. In this work, the atomistic-level interface effects are discussed along with a simple model to explain the results of the first-principles calculations. The guideline to design high-performance FTJs

————
[*]mshin@kaist.ac.kr

is suggested with keywords such as "interface dipoles," "polarized interfaces," and "atomistic asymmetry."

II. SIMULATION APPROACH

The density-functional-theory calculations are performed with the SIESTA package [28]. We use the generalized-gradient approximation for the exchange-correlation energy. The double-ζ polarized basis set is used, and an energy cutoff of 200 Ry is used for the calculations. Monkhorst-Pack k-point samplings of $10 \times 10 \times 10$ and $5 \times 5 \times 1$ is performed for the bulk and slab structures, respectively. The atoms are relaxed until the forces are smaller than 0.02 eV/Å. The calculated lattice constants of bulk orthorhombic HfO_2 are $a = 5.27$ Å, $b = 5.09$ Å, and $c = 5.10$ Å, and those for HZO are 5.31, 5.12, and 5.13 Å, which agree well with findings from previous studies [26,29]. For the metal electrodes, we chose TiN, which has been widely used in experimental studies. Since the spontaneous polarization of HfO_2 and HZO is oriented along the [001] direction, we construct the atomistic device structures of $TiN/HfO_2/TiN$ and $TiN/HZO/TiN$ with their cross-sectional planes normal to that direction. To minimize the lattice mismatch between TiN and the FE at the interfaces, the atomistic structures of TiN/FE/TiN consist of supercells of the size of $\sqrt{2}$ times the lattice constants along the a and b axes as constructed in previous work [29]. The in-plane lattice constants are fixed to those of the FE to keep intact the electronic structure of the FE and so tensile strain of about 10.0% and 10.7% is introduced to the TiN layer for the HfO_2 and HZO structures, respectively. The TiN layers in the slab structure significantly screen the electrostatic field along the [001] direction of the polarization but the dipole correction is considered nevertheless. To explore the dependence of the device performance on the atomic termination of HfO_2 and HZO, we consider of six cases, which include four symmetrically terminated structures and two asymmetrically terminated structures.

Previous theoretical studies reported that under an O-rich (O-poor) condition, the O-terminated (Hf-terminated) surface of a cubic phase of HfO_2 is stable [30,31]. The (001) surface of ferroelectric HfO_2 that we consider in this work has the same trends. Also, differently from the prediction from the theoretical studies, the ferroelectric phase of HfO_2 has been observed and it is affected by various fabrication conditions, such as the capping metal, dopant, and temperature [17,32,33]. Thus, the formation of Hf-terminated and O-terminated layers seems to be feasible. To investigate the dependence of the device performances on the terminated layer, we consider the cases of the O-terminated, Hf-terminated, and Zr-terminated structures.

For $TiN/HfO_2/TiN$, we consider the three cases where HfO_2 is terminated by O atoms (O-HfO_2-O), by Hf atoms
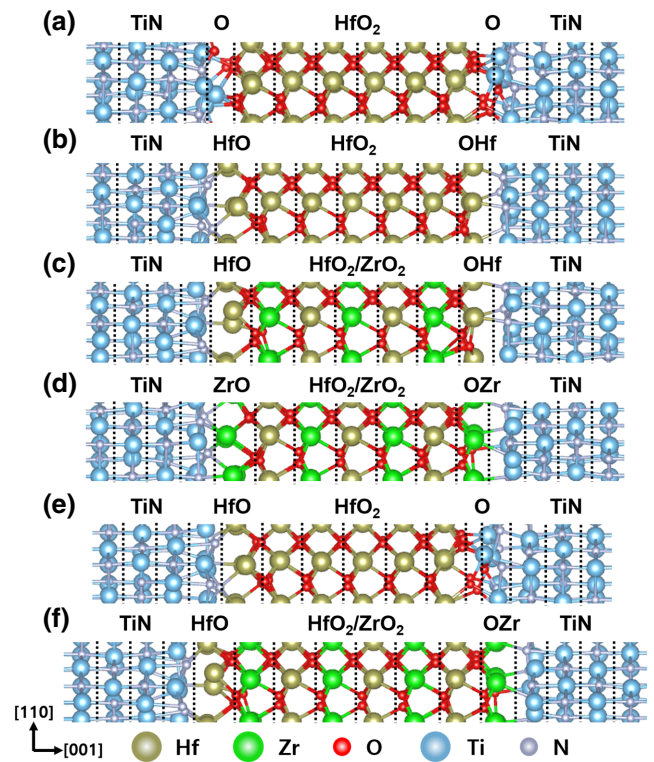

FIG. 1. The atomistic device structures with various terminated layers of TiN/FE/TiN FTJs. (a) O-HfO_2-O, (b) Hf-HfO_2-Hf, (c) Hf-HZO-Hf, (d) Zr-HZO-Zr, (e) Hf-HfO_2-O, and (f) Hf-HZO-Zr structures. (a)–(d) Symmetrically terminated structures and (e),(f) asymmetrically terminated structures.

(Hf-HfO_2-Hf), and by Hf and O atoms (Hf-HfO_2-O); see Figs. 1(a), 1(b), and 1(e).

For HZO where the HfO_2/ZrO_2 superlattice is formed, we consider the three cases where HZO is terminated by Hf atoms (Hf-HZO-Hf), by Zr atoms (Zr-HZO-Zr) at both junctions, and by Hf atoms at the left junction and Zr atoms at the right junction (Hf-HZO-Zr); see Figs. 1(c), 1(d), and 1(f). The structural information for the relaxed structures in Fig. 1 is provided as crystallographic information files in Supplemental Material [34]. The O-terminated cases are not considered in this work because the device performance is expected to be poor, as is clear in the following.

After relaxation of the atomistic device structures, we calculate the current-voltage characteristics using the nonequilibrium Green's function formalism implemented in the SIESTA package [28]. We use a 10×10 Monkhorst-Pack k grid for the current-voltage calculations in the transverse direction. The relaxed structures of TiN/FE/TiN are considered as the scattering region, and TiN semi-infinite electrodes are attached to the two ends of the structure for the current calculations.

III. ATOMISTIC INTERFACE EFFECTS

In this section, we describe a simple model of ours that is used to explain the simulation results in the next section. According to the model, there are three kinds of charges at the metal-FE junctions: the polarization surface charges and their screening charges, interface dipoles, and induced interface charges caused by O-atom displacement. The first ones are the usual macroscopic charges due to polarization, while the latter two are of atomistic origin; see Fig. 2.

Firstly, as O atoms are displaced from the center of the unit cell, the nonzero polarization is established across the FE and the usual polarization surface charges ρ_P and $-\rho_P$
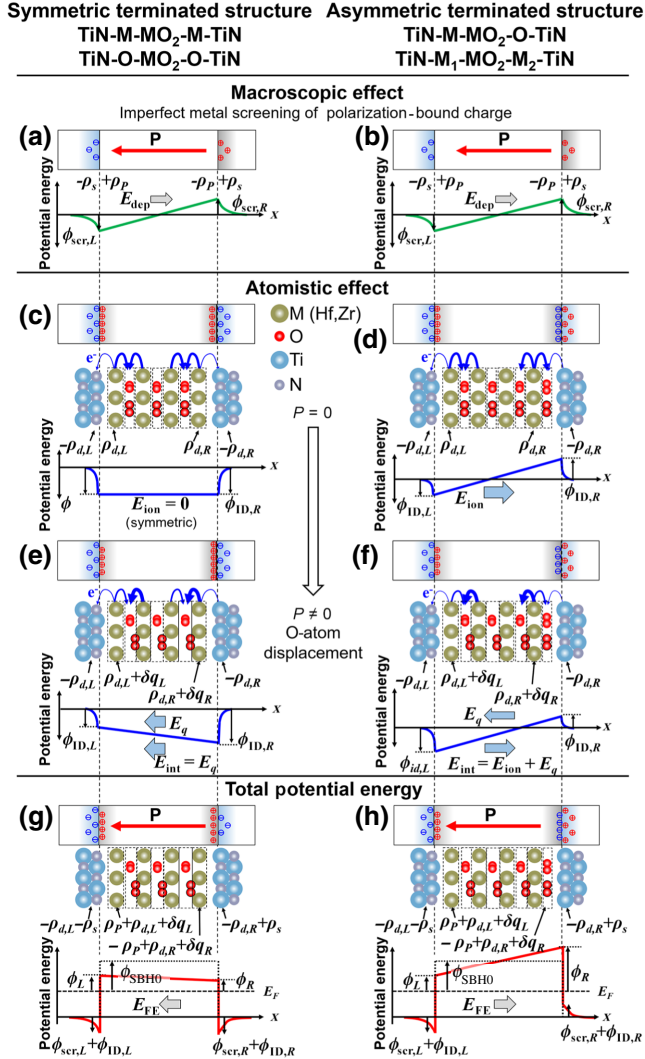

FIG. 2. Formation of the potential barrier depending on the terminated layers. (a),(c),(e),(g) The device with symmetrically terminated layers (the M-terminated case is shown). (b),(d),(f),(h) The device with asymmetrically terminated layers (the M- and O-terminated case is shown). In (c)–(f), the amount of charge transfer is schematically represented by the thickness of the curly arrows drawn on the top layer of the atoms.

appear on the FE side of the left and right junctions, respectively. On the metal side of the left and right junctions, screening charges of $-\rho_s$ and ρ_s, respectively, are induced; see Figs. 2(a) and 2(b).

Secondly, at $P = 0$, interface dipoles are induced at the terminated layers of the FE because HfO$_2$ is a polar material of which the charge of the terminated layers is nonzero; see Figs. 2(c) and 2(d). As the charges of the interfacial atoms in the FE are transferred to those of the metal electrodes, the terminating atoms at both ends of the FE assume nonzero charges of $\rho_{d,L}$ and $\rho_{d,R}$ at the left and right ends of the FE, respectively. The equal but opposite charges, $-\rho_{d,L}$ and $-\rho_{d,R}$, are attracted on the metal side of the junctions to form the dipoles.

Thirdly, because of O-atom displacement at $P \neq 0$, an extra amount of interface charge is induced in each of the terminated layers of the FE in addition to the interface dipoles; see Figs. 2(e) and 2(f). O atoms are shifted to the right for the polarization vector pointing to the left (P_L state), while they are shifted to the left for the polarization vector pointing to the right (P_R state). The displaced O atoms affect the charge of the terminating atoms such that it becomes more positive (negative) if O atoms move toward (away from) the terminating atoms. We denote δq_L and δq_R as the change of the charge of the terminating atoms relative to the case of $P = 0$. In our simple model, we assume $\delta q_R = -\delta q_L = \delta q$ and the screening charges on the metal side to screen δq are ignored.

Summarizing the above, the charge densities on the metal side of the left and right junctions are given as $\rho_{\mathrm{metal},L} = -\rho_{d,L} - \rho_s$ and $\rho_{\mathrm{metal},R} = -\rho_{d,R} + \rho_s$, respectively, while those on the FE side are $\rho_{\mathrm{FE},L} = \rho_P + \rho_{d,L} - \delta q$ and $\rho_{\mathrm{FE},R} = -\rho_P + \rho_{d,R} + \delta q$, respectively.

As shown in Figs. 2(g) and 2(h), the resultant height of the FE barrier is then given by

$$\phi_{L(R)} = \phi_{\mathrm{SBH0}} + \phi_{\mathrm{src},L(R)} + \phi_{\mathrm{ID},L(R)} \qquad (1)$$

where ϕ_{SBH0} is the difference between the work function of the metal and the electron affinity of the FE, ϕ_{scr} is the screening potential in the metal region, which is often given by Thomas-Fermi screening theory [2,35], and ϕ_{ID} is the potential due to the interface dipole, as explained further in the following.

As shown in Figs. 2(c) and 2(d), the electric fields induced by the interface dipoles have the effect of changing the tunnel barrier height by ϕ_{ID} [36–39]. For a negative polar interface ($\rho_d < 0$), such as the O-terminated layer, the tunnel barrier is raised ($\phi_{\mathrm{ID}} > 0$), while for a positively charged interface ($\rho_d > 0$), such as the Hf- and Zr-terminated layers, the barrier is lowered ($\phi_{\mathrm{ID}} < 0$). In particular, if the terminating atom species are different at the two junctions, interface dipoles of different magnitudes are induced. In such a case, an ionic built-in field (E_{ion})

[40] is established across the FE due to the asymmetric interface dipoles as shown in Fig. 2(d).

The total electric field (E_{FE}) established in the FE is then

$$E_{FE} = E_{FE0} + E_{int}, \qquad (2)$$

where

$$E_{FE0} = E_a + E_{bi} + E_{dep}, \qquad (3)$$

$$E_{int} = E_{ion} + E_q, \qquad (4)$$

where E_{FE0} is the usual macroscopic electric field across the FE, where E_a is the external field, E_{bi} is the built-in field due to the difference in the work functions of the left and right metal electrodes, and E_{dep} is the depolarization field. $E_{bi} = 0$ in this work because the same kind of metal is used for the left and right electrodes. We set $E_a = 0$ for the discussion in the following section. For simplicity, we assume that $|E_{dep}|$ is the same for the same combination of metal and FE, irrespective of the terminating atom species of the FE or the polarization directions, for E_{dep} is the quantity introduced at the macroscopic level. In Eq. (2), E_{int} is the electric field due to the charges at the atomistic interfaces, where E_{ion} is the built-in field mentioned previously and E_q is the electric field due to δq.

If we take the view that the FTJ is a macroscopic structure and ignore the atom-level details at the interfaces, E_{FE} would be equal to E_{FE0}. This is not the case for the FTJs considered in this work. As shown in the schematic diagram in Fig. 2, what we show in the next section as the key result of this paper is that $|E_{int}|$ can be comparable to or even bigger than $|E_{dep}|$. This means that if the terminating atom species are changed, different tunnel barrier heights and slopes can be established for the macroscopically same FTJ structure.

IV. RESULTS

Figures 3 and 4 show the layer-decomposed partial density of states of each of the symmetrically terminated structures (O-HfO$_2$-O, Hf-HfO$_2$-Hf, Hf-HZO-Hf, and Zr-HZO-Zr) and asymmetrically terminated structures (Hf-HfO$_2$-O and Hf-HZO-Zr), whose atomistic structures are shown in Fig. 1. There are three noticeable points: (i) the average barrier height sensitively depends on the atom species of the terminated layer; (ii) the electric field across the FE also depends on the interface atom species; (iii) a high *on:off* ratio is possible for asymmetrically terminated structure.

Firstly, it is observed that the tunnel barrier height sensitively depends on the atom species of the terminated layer. For HfO$_2$ FTJs, ϕ_L and ϕ_R are 1.87 and 2.46 eV for the O-terminated device, while they are 0.91 and 0.88 eV
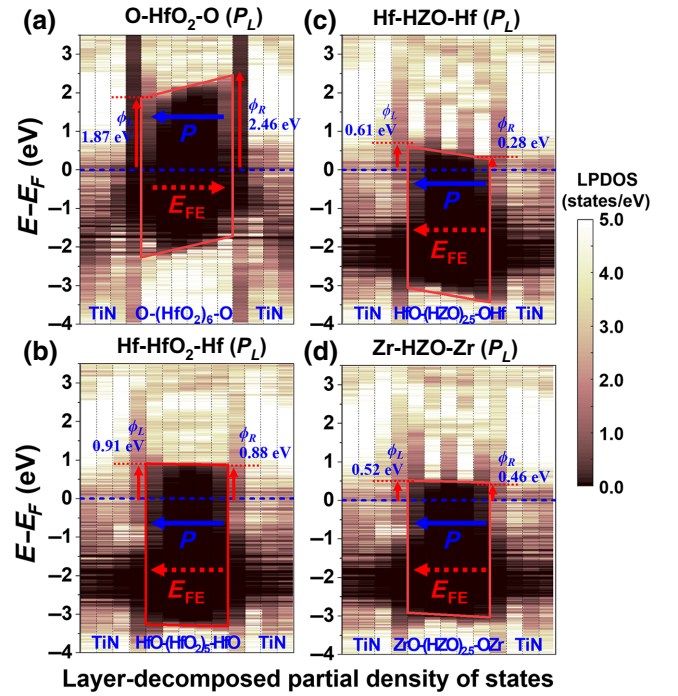

FIG. 3. Layered-decomposed partial density of states (LPDOS) for the symmetric interface structures (a) O-HfO$_2$-O, (b) Hf-HfO$_2$-Hf, (c) Hf-HZO-Hf, and (d) Zr-HZO-Zr. Solid blue and dotted red arrows indicate the polarization-direction and electric field direction, respectively. The dotted blue line represents the Fermi level shifted to 0.0 eV. ϕ_L and ϕ_R represent the barrier height at the left and right interfaces, respectively.

for the Hf-terminated device. For HZO FTJs, ϕ_L and ϕ_R are 0.61 and 0.28 eV for the Hf-terminated device, while they are 0.52 and 0.46 eV for the Zr-terminated device; see Figs. 3 and 4, where the polarization is in the P_L state. If we compare our values for the barrier height with those of other studies, the average barrier height of 2.16 eV for O-HfO$_2$-O is slightly higher than the 2.00 eV reported in a previous theoretical study [29]. The experimentally reported barrier height between undoped ferroelectric HfO$_2$ and TiN is not available in the literature, although a barrier height of 2.5 eV was measured in monoclinic HfO$_2$ (a high-*k* dielectric) [41]. The experimental barrier height between TiN and HZO was reported to lie in the range from about 1.2 to 2.3 eV [15,22], which is higher than our calculated value.

The dependence of the barrier height on the terminating atom species can be readily explained by the interface charges in Sec. III. To examine the charge properties on the basis of the model described in Sec. III, we calculate the number of excess charges using Bader charge analysis [42]: we subtract the valence charges from the total charges. Figure 5 shows the excess atomic charge near the interfaces. On the basis of the model in Sec. III, we extract
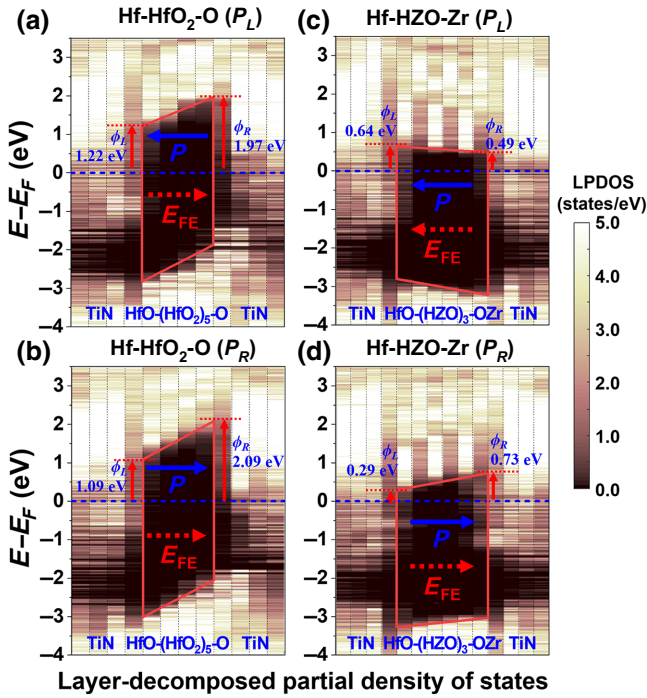
FIG. 4. Layered-decomposed partial density of states (LPDOS) for the asymmetric interface structures of (a),(b) Hf-HfO$_2$-O and (c),(d) Hf-HZO-Zr for P_L and P_R states. Solid blue and dotted red arrows indicate the polarization-direction and electric field direction, respectively. The dotted blue line represents the Fermi level shifted to 0.0 eV.

the charge components of ρ_d, ρ_s, and δq from excess charges of terminated layers in the symmetric structures as follows: $\rho_d = (Q_{M,R} + Q_{M,L})/2$, $\rho_s = (Q_{M,R} - Q_{M,L})/2$, and $\delta q = (Q_{FE,R} - Q_{FE,L})/2$, where $Q_{M,R}$ ($Q_{M,L}$) and $Q_{FE,R}$ ($Q_{FE,L}$) are the excess atomic charges of the metal region and the terminated layers, respectively, at the right (left) side; see Table I. From Fig. 5 and Table I, it is seen that the Hf-terminated or Zr-terminated structure has a positive polar interface of $\rho_d > 0$, while the O-terminated structure has a negative polar interface of $\rho_d < 0$. This accounts for the results in Figs. 3 and 4 that the barrier height of the former is noticeably lower than that of the latter.

As the second key result of this work, we find that the total electric field E_{FE} across the FE is sensitively dependent on the atom species of the terminated layers and its direction can even be reversed due to the interface charges. In Figs. 3(a) and 3(b), for the same TiN/HfO$_2$/TiN FTJ and for the same polarization state of P_L, the magnitudes of E_{FE} are quite different between the O-HfO$_2$-O and Hf-HfO$_2$-Hf structures and the directions are opposite. It is especially remarkable that for the latter structure the direction of E_{FE} is opposite that of E_{dep}, which is contrary to common knowledge that E_{FE} is equal to E_{dep} in a

ferroelectric material if the external field and built-in field are absent.

The reversal of E_{FE} is more pronounced in HZO FTJs as is seen in Figs. 3(c) and 3(d). E_{FE} of the Hf-HZO-Hf and Zr-HZO-Zr structures points to the left, which is the same direction as the polarization state of P_L, with the Hf-HZO-Hf structure showing the steeper barrier.

The above results can be explained by the contribution of E_{int} of Eqs. (2) and (4) and the associated interface charges shown in Figs. 5(a) and 5(b). From the Figs. 5(a) and 5(b), it is seen that the difference between $\rho_{FE,L}$ and $\rho_{FE,R}$ of Hf-HfO$_2$-Hf is larger than that of O-HfO$_2$-O. This is because the extracted δq of $0.204e$ of the Hf-terminated layer is larger than the $0.0898e$ of the O-terminated layer; see Table I. This means that according to our model described in the previous section [see Fig. 2(e)], δq of the Hf-terminated structure is not only larger than that of the O-terminated structure but also large enough to over-compensate E_{dep}, making the total field E_{FE} in the former structure smaller in terms of its magnitude but opposite in its direction.

The same applies to Hf-terminated and Zr-terminated structures of HZO FTJs, where the former shows stronger E_{FE} than the latter. In Figs. 5(c) and 5(d) and Table I, it is seen that δq of $0.171e$ of Hf-HZO-Hf is larger than the $0.137e$ of Zr-HZO-Zr, which explains the fact that the former shows a steeper tunnel barrier due to stronger E_q.

As the third and the most-important result of this work, we find that a high *on*:*off* current ratio of more than 10 can be achieved in the asymmetrically terminated structure, which is the structure with different atom species at the two terminated FE layers. We first consider the layer-decomposed partial density of states of Hf-HfO$_2$-O and Hf-HZO-Zr in Fig. 4. For the asymmetrically terminated structure of Hf-HfO$_2$-O, ϕ_L and ϕ_R of the P_L state are 1.22 and 1.97 eV, but these values are not simply reversed on reversal of the polarization direction to the P_R state. They are 1.09 and 2.09 eV for the P_R state. For Hf-HZO-Zr, ϕ_L and ϕ_R are 0.64 and 0.49 eV for P_L and 0.29 and 0.73 eV for P_R; see Figs. 4(c) and 4(d).

In the asymmetrically terminated structures, E_{ion} , which is the electric field due to the asymmetric dipoles at the

TABLE I. The charge components dependent on the atom species of the terminated layer extracted from the model in Sec. III. The values represent the average per atom.

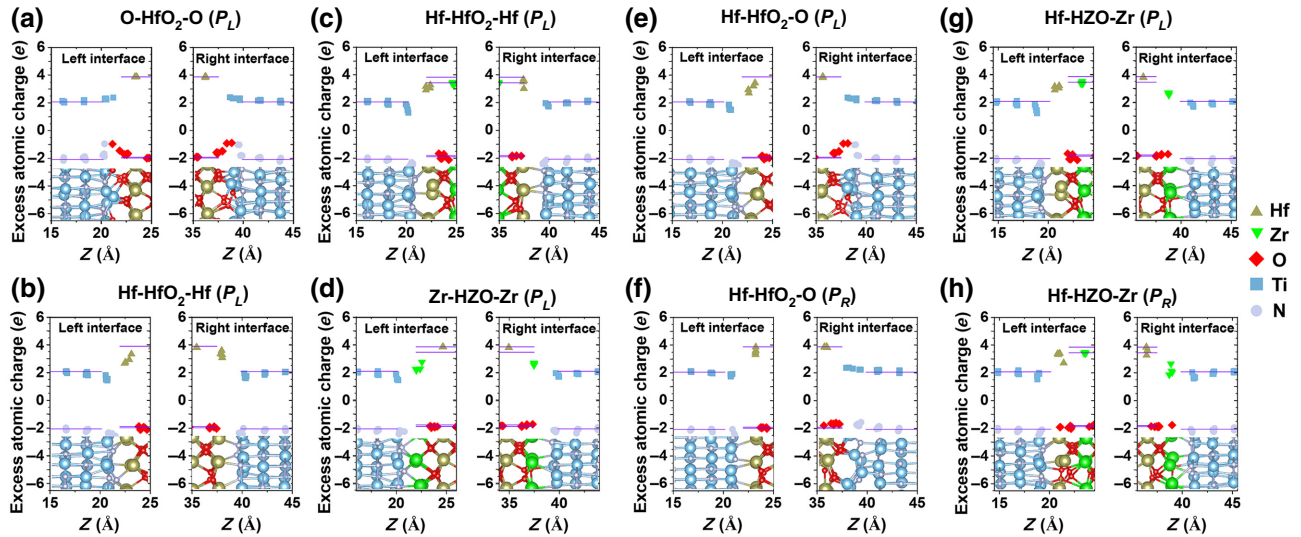|	HfO$_2$		HZO	
	O terminated	Hf terminated	Hf terminated	Zr terminated
ρ_d	$-0.879e$	$0.901e$	$0.906e$	$0.623e$
ρ_s	$0.109e$	$0.132e$	$0.180e$	$0.164e$
$|\delta q|$	$0.0898e$	$0.204e$	$0.171e$	$0.137e$

FIG. 5.   Excess atomic charge for symmetric structures (a) O-HfO$_2$-O, (b) Hf-HfO$_2$-Hf, (c) Hf-HZO-Hf, and (d) Zr-HZO-Zr and asymmetric structures (e),(f) Hf-HfO$_2$-O and (g),(h) Hf-HZO-Zr . The solid lines represent the atomic charges in the bulk TiN, HfO$_2$, and HZO. The atomic charges are calculated Bader charge analysis.

two terminated layers, plays the same role as the built-in electric field E_{bi}. This component is shown in Fig. 2(d). Much as $E_{bi} \neq 0$ for asymmetrical metal electrodes, where the left and right electrodes are made of the different metals with different work functions, $E_{ion} \neq 0$ for asymmetrically terminated structures. The former is extrinsic, while the latter is intrinsic.

For both Hf-HfO$_2$-O and Hf-HZO-Zr, E_{ion} is directed to the right since $\rho_{d,L} > 0 > \rho_{d,R}$ for the former and $\rho_{d,L} > \rho_{d,R} > 0$ for the latter; see Figs. 5(e) and 5(g). As shown in Table I, ρ_d of the O-terminated Hf-terminated layer of HfO$_2$ is negative (positive) and ρ_d of the Hf-terminated layer of HZO is more positively charged than that of the Zr-terminated layer of HZO. In the case of Hf-HfO$_2$-O, the direction of E_{FE} is not changed on reversal of the polarization. This is because relatively strong E_{ion} due to the relatively large difference between positive $\rho_{d,L}$ and negative $\rho_{d,R}$ gives the dominant contribution to E_{FE}. That is, $|E_{ion}| > |E_{dep} + E_q|$. The interface dipoles are not reversed by the polarization reversal and hence E_{ion} is not reversed. For Hf-HZO-Zr, both $\rho_{d,L}$ and $\rho_{d,R}$ are positive and so E_{ion} is not as strong, resulting in the reversal of E_{FE} on reversal of the polarization.

Figures 6(a) and 6(b) show the calculated current and *on*:*off* current ratio of Hf-HfO$_2$-O and Hf-HZO-Zr. What is remarkable is the high *on*:*off* ratio of more than 1 in the asymmetrically terminated devices as compared with the symmetrically terminated devices. In particular, the ratio reaches as high as 12 for Hf-HZO-Zr. The implication of this result is significant because a high current ratio can be possible without dissimilar metal electrodes or without additional composite layers to build asymmetric tunnel barriers.

As explained above, the polar interfaces and E_{ion} play a critical role in the asymmetrically terminated structures. For Hf-HfO$_2$-O, the negatively charged O-terminated interface brings about a relatively high tunnel barrier and high E_{ion}, limiting the performance of the FTJ in the range of the external voltage considered in this work. For Hf-HZO-Zr with positively charged polar interfaces at both junctions, on the other hand, the average tunnel barrier height is low and a transition between high and low barriers is allowed by the polarization reversal, making a high *on*:*off* ratio possible with the help of E_{ion}. In the structure, the "high" current is achieved by the Fowler-Nordheim tunneling in the *on* state, while the "low" current is due to the direct tunneling through the higher barrier in the *off* state.
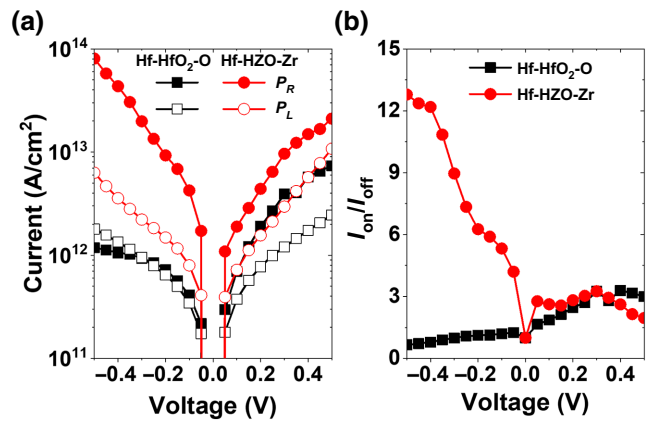

FIG. 6.   (a) Current-voltage characteristics and (b) the *on*:*off* current ratio for FTJs with asymmetric atomistic structures of Hf-HfO$_2$-O and Hf-HZO-Zr.

V. DISCUSSION

In a FTJ, to achieve a high *on*:*off* current ratio significant modulation of the tunnel barrier should be allowed by the polarization reversal. That is, the degree of the barrier modulation should be such that the Fowler-Nordheim tunneling current should flow through the steep barrier in the *on* state but it must be blocked by the high barrier in the *off* state. We find in this work that the atomistic interface effect can be so great that it can sufficiently modulate the barrier height and thus E_{FE}. We showed in the previous section that, depending on what kind of atomic species there are at the metal-FE junctions, the tunnel barrier height can be radically changed. In particular, we find that in the comparison between the O-HfO$_2$-O and Hf-HfO$_2$-Hf structures, E_{int} induced by interfacial charges can overcompensate E_{dep}, leading to the different E_{FE} between them. As a consequence, vastly different *on*:*off* current ratios can be provided in the otherwise same FTJ structure.

From the point of view of device performance, the presence of the interface charges and hence E_q is undesirable because it weakens E_{FE} (E_q is in the opposite direction to E_{dep}). However, by having positively polarized, asymmetrically terminated interfaces to lower the average barrier height and to have an effective built-in field, one can achieve a high *on*:*off* current ratio, as demonstrated above for the case of the Hf-HZO-Zr structure.

There have been experimental reports [15,23] that although the device structure is symmetric, the tunnel barrier is not symmetrically modulated with the polarization. We speculate that this may be due to the formation of asymmetrical interfaces during the fabrication processes where the oxygen concentrations at the interfaces influence the interfacial charges. Also, the atomistic arrangement at and near the interfaces can affect the interface dipole as well as the interface charges. The TiO$_{1-x}$N$_x$ interfacial layer is formed by O atoms mixed into the TiN layer. This layer affects the effective screening length of the metal electrodes [15] and its disordered chemical bonding at the interface can create a small interface dipole [43], possibly contributing to E_{int}.

Spin properties in ferroelectric materials are one of the important properties to enable multifunctionality of FTJs [44,45]. It has been reported that the spin-orbit coupling of HfO$_2$ induces a large band split [46]. A theoretical study has also predicted a large tunneling anomalous Hall effect in FTJs with its large spin-orbit coupling [47]. Although we focus on the properties of the tunnel barrier depending on the terminated layers of HfO$_2$, further work is needed with regard to these effects.

VI. CONCLUSION

In summary, we perform first-principles calculations to investigate HfO$_2$-based FTJs at the atomistic level. We find

that, depending on the terminating atom species of ferroelectric layer, different tunnel barrier heights and profiles can be built in otherwise the same FTJ structure. The interface dipoles formed at the two junctions play a critical role, and the tunnel barrier height can be raised or lowered according to the polarity of the interface. The asymmetrical interface dipoles establish an effective built-in electric field, which can help achieve a high *on*:*off* current ratio at low external voltages.

The guideline for high device performance is then to ensure one has positively polarized, asymmetrically terminated interfaces to lower the average barrier height and to induce an effective built-in field. We demonstrate that the HZO FTJ structure which is asymmetrically terminated with Hf and Zr atoms shows an *on*:*off* ratio of 12. Our theoretical results may shed light on atomistic-level processes for the fabrication of high-performance FTJ devices with applications such as neuromorphic and nonvolatile-memory devices.

[1] E. Y. Tsymbal and H. Kohlstedt, Tunneling across a ferroelectric, Science **313,** 181 (2006).

[2] M. Y. Zhuravlev, R. F. Sabirianov, S. S. Jaswal, and E. Y. Tsymbal, Giant Electroresistance in Ferroelectric Tunnel Junctions, Phys. Rev. Lett. **94,** 1 (2005).

[3] A. Chanthbouala, V. Garcia, R. O. Cherifi, K. Bouze-houane, S. Fusil, X. Moya, S. Xavier, H. Yamada, C. Deranlot, N. D. Mathur, M. Bibes, A. Barthélémy, and J. Grollier, A ferroelectric memristor, Nat. Mater. **11,** 860 (2012).

[4] S. Majumdar, H. Tan, Q. H. Qin, and S. van Dijken, Energy-efficient organic ferroelectric tunnel junction memristors for neuromorphic computing, Adv. Electron. Mater. **5,** 1 (2019).

[5] Z. Wen and D. Wu, Ferroelectric tunnel junctions: Modulations on the potential barrier, Adv. Mater. **1904123,** 1 (2019).

[6] L. L. Tao and J. Wang, Ferroelectricity and tunneling electroresistance effect in asymmetric ferroelectric tunnel junctions, J. Appl. Phys. **119,** 224104 (2016).

[7] X. Liu, J. D. Burton, and E. Y. Tsymbal, Enhanced Tunneling Electroresistance in Ferroelectric Tunnel Junctions due to the Reversible Metallization of the Barrier, Phys. Rev. Lett. **116,** 3 (2016).

[8] B. Max, M. Hoffmann, S. Slesazeck, and T. Mikolajick, Ferroelectric tunnel junctions based on ferroelectric-dielectric Hf$_{0.5}$Zr$_{0.5}$O$_2$/Al$_2$O$_3$ capacitor stacks, Eur. Solid-State Device Res. Conf. **2018,** 142 (2018).

[9] A. Gruverman, D. Wu, H. Lu, Y. Wang, H. W. Jang, C. M. Folkman, M. Y. Zhuravlev, D. Felker, M. Rzchowski, C. B.

Eom, and E. Y. Tsymbal, Tunneling electroresistance effect in ferroelectric tunnel junctions at the nanoscale, Nano Lett. 9, 3539 (2009).

[10] H. S. Lee, W. Han, H. Y. Chung, M. Rozenberg, K. Kim, Z. Lee, G. Y. Yeom, and H. H. Park, Ferroelectric tunnel junction for dense cross-point arrays, ACS Appl. Mater. Interfaces 7, 22348 (2015).

[11] S. Boyn, A. M. Douglas, C. Blouzon, P. Turner, A. Barthélémy, M. Bibes, S. Fusil, J. M. Gregg, and V. Garcia, Tunnel electroresistance in BiFeO$_3$ junctions: Size does matter, Appl. Phys. Lett. 109, 232902 (2016).

[12] T. S. Böscke, J. Müller, D. Bräuhaus, U. Schröder, and U. Böttger, Ferroelectricity in hafnium oxide thin films, Appl. Phys. Lett. 99, 102903 (2011).

[13] T. Mittmann, F. P. Fengler, C. Richter, M. H. Park, T. Mikolajick, and U. Schroeder, Optimizing process conditions for improved Hf$_{1-x}$Zr$_x$O$_2$ ferroelectric capacitor performance, Microelectron. Eng. 178, 48 (2017).

[14] X. Tian, S. Shibayama, T. Nishimura, T. Yajima, S. Migita, and A. Toriumi, Evolution of ferroelectric HfO$_2$ in ultrathin region down to 3 nm, Appl. Phys. Lett. 112, 102902 (2018).

[15] Y. Matveyev, D. Negrov, A. Chernikova, Y. Lebedinskii, R. Kirtaev, S. Zarubin, E. Suvorova, A. Gloskovskii, and A. Zenkevich, Effect of polarization reversal in ferroelectric TiN/Hf$_{0.5}$Zr$_{0.5}$O$_2$/TiN devices on electronic conditions at interfaces studied in operando by hard X-ray photoemission spectroscopy, ACS Appl. Mater. Interfaces 9, 43370 (2017).

[16] S. J. Kim, J. Mohan, S. R. Summerfelt, and J. Kim, Ferroelectric Hf$_{0.5}$Zr$_{0.5}$O$_2$ thin films: A review of recent advances, Jom 71, 246 (2019).

[17] S. J. Kim, D. Narayan, J. G. Lee, J. Mohan, J. S. Lee, J. Lee, H. S. Kim, Y. C. Byun, A. T. Lucero, C. D. Young, S. R. Summerfelt, T. San, L. Colombo, and J. Kim, Large ferroelectric polarization of TiN/Hf$_{0.5}$Zr$_{0.5}$O$_2$/TiN capacitors due to stress-induced crystallization at low thermal budget, Appl. Phys. Lett. 111, 242901 (2017).

[18] S. Fujii, Y. Kamimuta, T. Ino, Y. Nakasaki, R. Takaishi, and M. Saitoh, First demonstration and performance improvement of ferroelectric HfO$_2$-based resistive switch with low operation current and intrinsic diode property, Dig. Tech. Pap. – Symp. VLSI Technol. 2016, 2 (2016).

[19] X. Tian and A. Toriumi, in *2017 IEEE Electron Devices Technol. Manuf. Conf. EDTM 2017 – Proc.* (IEEE, Toyama, Japan, 2017), p. 63.

[20] F. Ambriz-Vargas, G. Kolhatkar, M. Broyer, A. Hadj-Youssef, R. Nouar, A. Sarkissian, R. Thomas, C. Gomez-Yáñez, M. A. Gauthier, and A. Ruediger, A complementary metal oxide semiconductor process-compatible ferroelectric tunnel junction, ACS Appl. Mater. Interfaces 9, 13262 (2017).

[21] M. Kobayashi, Y. Tagawa, F. Mo, T. Saraya, and T. Hiramoto, Ferroelectric HfO$_2$ tunnel junction memory with high TER and multi-level operation featuring metal replacement process, IEEE J. Electron Devices Soc. 7, 158 (2019).

[22] J. Yoon, S. Hong, Y. W. Song, J. H. Ahn, and S. E. Ahn, Understanding tunneling electroresistance effect through

potential profile in Pt/Hf$_{0.5}$Zr$_{0.5}$O$_2$/TiN ferroelectric tunnel junction memory, Appl. Phys. Lett. 115, 153502 (2019).

[23] F. Ambriz-Vargas, G. Kolhatkar, R. Thomas, R. Nouar, A. Sarkissian, C. Gomez-Yáñez, M. A. Gauthier, and A. Ruediger, Tunneling electroresistance effect in a Pt/Hf$_{0.5}$Zr$_{0.5}$O$_2$/Pt structure, Appl. Phys. Lett. 110, 093106 (2017).

[24] Q. Yang, L. Tao, Y. Zhang, M. Li, Z. Jiang, E. Y. Tsymbal, and V. Alexandrov, Ferroelectric tunnel junctions enhanced by a polar oxide barrier layer, Nano Lett. 19, 7385 (2019).

[25] M. Li, L. L. Tao, J. P. Velev, and E. Y. Tsymbal, Resonant tunneling across a ferroelectric domain wall, Phys. Rev. B 97, 1 (2018).

[26] R. Materlik, C. Kunneth, and A. Kersch, The origin of ferroelectricity in Hf$_{1-x}$Zr$_x$O$_2$: A computational investigation and a surface energy model, J. Appl. Phys. 117, 134109 (2015).

[27] J. Müller, T. S. Böscke, U. Schröder, S. Mueller, D. Bräuhaus, U. Böttger, L. Frey, and T. Mikolajick, Ferroelectricity in simple binary ZrO$_2$ and HfO$_2$, Nano Lett. 12, 4318 (2012).

[28] J. M. Soler, E. Artacho, J. D. Gale, A. García, J. Junquera, P. Ordejón, and D. Sánchez-Portal, The SIESTA method for *abinitio* order-N materials simulation, J. Phys. Condens. Matter 14, 2745 (2002).

[29] K. H. Xue, H. L. Su, H. Li, H. J. Sun, W. F. He, T. C. Chang, L. Chen, D. W. Zhang, and X. S. Miao, Model of dielectric breakdown in hafnia-based ferroelectric capacitors, J. Appl. Phys. 124, 024103 (2018).

[30] G. H. Chen, Z. F. Hou, and X. G. Gong, Structural and electronic properties of cubic HfO$_2$ surfaces, Comput. Mater. Sci. 44, 46 (2008).

[31] K. Y. Tse, D. Liu, and J. Robertson, Electronic and atomic structure of metal-HfO$_2$ interfaces, Phys. Rev. B – Condens. Matter Mater. Phys. 81, 1 (2010).

[32] G. Karbasian, R. Dos Reis, A. K. Yadav, A. J. Tan, C. Hu, and S. Salahuddin, Stabilization of ferroelectric phase in tungsten capped Hf$_{0.8}$Zr$_{0.2}$O$_2$, Appl. Phys. Lett. 111, 093106 (2017).

[33] S. Starschich and U. Boettger, An extensive study of the influence of dopants on the ferroelectric properties of HfO$_2$, J. Mater. Chem. C 5, 333 (2017).

[34] See Supplemental Material at http://link.aps.org/supplemental/10.1103/PhysRevApplied.14.054018 for the structural details in the crystallographic information files for Fig. 1.

[35] S. C. Chang, A. Naeemi, D. E. Nikonov, and A. Gruverman, Theoretical Approach to Electroresistance in Ferroelectric Tunnel Junctions, Phys. Rev. Appl. 7, 1 (2017).

[36] R. T. Tung, Formation of an electric dipole at metal-semiconductor interfaces, Phys. Rev. B – Condens. Matter Mater. Phys. 64, 1 (2001).

[37] Y. Nishi, T. Yamauchi, T. Marukame, A. Kinoshita, J. Koga, and K. Kato, Schottky barrier height modulation by atomic dipoles at the silicide/silicon interface, Phys. Rev. B – Condens. Matter Mater. Phys. 84, 3 (2011).

[38] R. T. Tung, The physics and chemistry of the Schottky barrier height, Appl. Phys. Rev. 1, 011304 (2014).

[39] T. Yajima, Y. Hikita, M. Minohara, C. Bell, J. A. Mundy, L. F. Kourkoutis, D. A. Muller, H. Kumigashira, M. Oshima, and H. Y. Hwang, Controlling band alignments by artificial interface dipoles at perovskite heterointerfaces, Nat. Commun. **6**, 1 (2015).

[40] G. Singh-Bhalla, C. Bell, J. Ravichandran, W. Siemons, Y. Hikita, S. Salahuddin, A. F. Hebard, H. Y. Hwang, and R. Ramesh, Built-in and induced polarization across $LaAlO_3/SrTiO_3$ heterojunctions, Nat. Phys. **7**, 80 (2011).

[41] S. Cimino, A. Padovani, L. Larcher, V. V. Afanas'Ev, H. J. Hwang, Y. G. Lee, M. Jurczac, D. Wouters, B. H. Lee, H. Hwang, and L. Pantisano, A study of the leakage current in $TiN/HfO_2/TiN$ capacitors, Microelectron. Eng. **95**, 71 (2012).

[42] G. Henkelman, A. Arnaldsson, and H. Jónsson, A fast and robust algorithm for Bader decomposition of charge density, Comput. Mater. Sci. **36**, 354 (2006).

[43] N. Miyata, Electric-field-controlled interface dipole modulation for Si-based memory devices, Sci. Rep. **8**, 1 (2018).

[44] E. Y. Tsymbal, A. Gruverman, V. Garcia, M. Bibes, and A. Barthélémy, Ferroelectric and multiferroic tunnel junctions, MRS Bull. **37**, 138 (2012).

[45] D. Pantel, S. Goetze, D. Hesse, and M. Alexe, Reversible electrical switching of spin polarization in multiferroic tunnel junctions, Nat. Mater. **11**, 289 (2012).

[46] L. L. Tao, T. R. Paudel, A. A. Kovalev, and E. Y. Tsymbal, Reversible spin texture in ferroelectric HfO_2, Phys. Rev. B **95**, 1 (2017).

[47] M. Y. Zhuravlev, A. Alexandrov, L. L. Tao, and E. Y. Tsymbal, Tunneling anomalous Hall effect in a ferroelectric tunnel junction, Appl. Phys. Lett. **113**, 172405 (2018).